

Chemical physics of superconductivity in layered yttrium carbide halides from first principles

Ryosuke Akashi,^{1,*} Ryotaro Arita^{1b,2,3} Chao Zhang^{1b,4} K. Tanaka^{1b,5} and J. S. Tse⁵

¹*Department of Physics, The University of Tokyo, Hongo, Bunkyo-ku, Tokyo 113-0033, Japan*

²*RIKEN Center for Emergent Matter Science, Wako, Saitama 351-0198, Japan*

³*Department of Applied Physics, The University of Tokyo, Hongo, Bunkyo-ku, Tokyo 113-8656, Japan*

⁴*Department of Physics, Yantai University, Yantai 264005, China*

⁵*Department of Physics and Engineering Physics, University of Saskatchewan, 116 Science Place, Saskatoon, Saskatchewan, Canada S7N 5E2*



(Received 24 February 2021; revised 8 April 2021; accepted 8 April 2021; published 29 April 2021)

We perform a thorough first-principles study on superconductivity in yttrium carbide halide $Y_2X_2C_2$ ($X = \text{Cl, Br, I}$) whose maximum transition temperature (T_c) amounts to ~ 10 K. A detailed analysis on the optimized crystal structures reveals that the Y_2C_2 blocks are compressed uniaxially upon the halogen substitution from Cl, Br to I, contrary to the monotonic expansion of the lattice vectors. With a nonempirical method based on the density functional theory for superconductors within the conventional phonon mechanism, we successfully reproduce the halogen dependence of T_c . An anomalously enhanced coupling of one C_2 libration mode is observed in $Y_2I_2C_2$, which implies a possible departure from the conventional pairing picture. Utilizing the Wannier representation of the electron-phonon coupling, we show that the halogen electronic orbitals and ionic vibrations scarcely contribute to the superconducting pairing. The halogen dependence of this system is hence an indirect effect of the halogen ions through the uniaxial compressive force on the superconducting Y_2C_2 blocks. We thus establish a quantitatively reliable picture of the superconducting physics of this system, extracting a unique effect of the atomic substitution which is potentially applicable to other superconductors.

DOI: [10.1103/PhysRevB.103.134517](https://doi.org/10.1103/PhysRevB.103.134517)

I. INTRODUCTION

Synthesizing high-temperature superconductors by design has been a long-sought goal of materials physics and chemistry. Investigating light element compounds is a rational strategy derived from the Bardeen-Cooper-Schrieffer theory of phonon-mediated superconductivity [1,2], where the transition temperature T_c is proportional to the frequency of phonons mediating the electron pairing. The recent predictions [3–5] and later (or almost concurrent) discoveries [6–8] of hydride superconductors under pressure is a milestone of the theory, which was finally brought about by the advance of the first-principles electronic structure calculation and crystal structure prediction methods [9,10].

In this context, carbon compounds have also long been a subject of intense study. Owing to the relatively small mass and strong covalent bonding of carbon atoms, they may host high-frequency phonons. Among them, the rare-earth carbides Re_2C_3 ($Re = \text{rare earth}$) (Refs. [11–13]), ReC_2 (Refs. [14,15]), and carbide halide $Re_2X_2C_2$ (Refs. [16,17]) are interesting materials. They generally show superconductivity at temperatures around ~ 10 K; especially in the sesquicarbide T_c reaches 18 K at ambient pressure [13]. Remarkably, they contain carbon dimers in their crystal structures. From the physics viewpoint, these materials are attractive as they can be model systems where T_c is boosted by the high frequency vibrations of the carbon dimers. On

the other hand, from the chemistry viewpoint, their formula units are significant since the valence electrons cannot be straightforwardly attributed to the constituent atoms from their regular ionic valence. According to the Zintl-Klemm concept, each carbon dimer should host additional valence electrons and exist as a molecular anion $(C_2)^{-n}$. Inspired by these characteristics, a “chemical” theory of superconductivity for this system has been proposed: The superconducting pairing occurs locally at the dimer sites, where extra electrons are confined as a consequence of the Zintl-Klemm rule [18]. Superconductivity in the rare-earth carbides thus serves an interesting intersection of physics and chemistry.

In this work, we conduct a first-principles study of the electronic, phononic and superconducting properties of the yttrium carbide halide $Y_2X_2C_2$ ($X = \text{Cl, Br, I}$) to establish its chemical-physical description. This system becomes superconducting with $T_c \sim 11.6$ K at maximum [16,19,20]. A distinguished feature of this system is its two-dimensional layered crystal structure, where the yttrium blocks containing the carbon dimers and intercalant halogen blocks are alternately stacked. Substitution of the halogen atoms yields systematic change of T_c from ~ 2.5 K ($X = \text{Cl}$) to 5.0 (Br) and 10 K (I) [16]. The electron-phonon coupling properties in some related materials such as Y_2C_3 (Ref. [21]) and YC_2 (Ref. [22]) have been studied with the first-principles calculations, and found that the mechanism conforms to the conventional phonon-mediated superconducting theory. For the carbide halide, calculations of its electronic band structure and Raman-active modes have been reported [23], but the electron-phonon and superconducting calculations are yet

*ryosuke.akashi@phys.s.u-tokyo.ac.jp

unprecedented. Also, a perspective on the halogen dependence is lacking since the study on the low- T_c chloride is scarce. Actually the carbon isotope effect in this system is not as evident as in the other yttrium carbides [24]: The two-dimensional structure specific to the carbide halide may induce some anomaly beyond the conventional phonon pairing mechanism.

We report thorough first-principles calculations of the electron-phonon coupling to examine whether the experimentally observed superconducting transition temperatures can be reasonably explained within the conventional phonon-mediated scenario. From the optimized crystal structures, we find an effect of the halogen ions as a source of local pressure on the superconducting Y_2C_2 layers. Using the Wannier representation of the electron-phonon coupling matrix elements, we disentangle the interplay of the atomic orbitals, through which a chemical view on the superconducting electronic states is developed. The pioneering local Zintl-Klemm pairing theory [18] is finally found to be not as relevant as expected. The superconducting transition temperatures are evaluated nonempirically with the density functional theory for superconductors (SCDFT), with which the halogen atom dependence of T_c is well reproduced. A possible departure from the conventional pairing scenario is also suggested in $Y_2I_2C_2$, which exhibits the highest T_c among the stoichiometric $Y_2X_2C_2$ series.

II. METHOD AND COMPUTATIONAL DETAILS

We calculated the electronic and phononic properties of $Y_2X_2C_2$ ($X = Cl, Br, I$) from first principles with the plane-wave pseudopotential method implemented in QUANTUM ESPRESSO [25]. We solved the normal-state Kohn-Sham equation [26,27] for the electronic normal state and later analysis of the phonon and superconducting states. The Troullier-Martins norm-conserving pseudopotentials [28] for the Y, C, and halogen atoms were employed. The Perdew-Burke-Ernzerhof generalized gradient approximation for solids (PBEsol) [29] was used for the exchange-correlation functional. The phononic properties were calculated with the density functional perturbation theory [30] as implemented in the PH.X package.

We examine the pairing characteristics within the conventional Eliashberg theory [31–33] of phonon-mediated superconductivity with the Migdal approximation [34]. We calculate the Eliashberg spectral function $\alpha^2F(\omega)$ [32], which represents the electron-phonon coupling strength for the pairing

$$\alpha^2F(\omega) = \frac{1}{N(0)} \sum_{\nu\mathbf{q}} \sum_{n'n\mathbf{k}} |g_{n\mathbf{k}+\mathbf{q},n'\mathbf{k}}^{\nu\mathbf{q}}|^2 \delta(\omega - \omega_{\nu\mathbf{q}}) \times \delta(\xi_{n\mathbf{k}+\mathbf{q}}) \delta(\xi_{n'\mathbf{k}}). \quad (1)$$

The electronic Kohn-Sham and phononic vibrational eigenstates are labeled by the band index n (n'), electronic wave vector \mathbf{k} , mode index ν and phonon wave vector \mathbf{q} , respectively. $\xi_{n\mathbf{k}}$ denotes the normal-state Kohn-Sham energy eigenvalue measured from the Fermi level. $\omega_{\nu\mathbf{q}}$ is the phonon frequency. $N(\xi)$ denotes the electronic density of states (DOS). The electron-phonon coupling coefficient $g_{n\mathbf{k}+\mathbf{q},n'\mathbf{k}}^{\nu\mathbf{q}}$ is

defined as the matrix element between the Kohn-Sham states

$$g_{n\mathbf{k}+\mathbf{q},n'\mathbf{k}}^{\nu\mathbf{q}} = \langle n\mathbf{k} + \mathbf{q} | \partial_{\nu\mathbf{q}} V_{KS} | n'\mathbf{k} \rangle, \quad (2)$$

where $\partial_{\nu\mathbf{q}} V_{KS}$ denotes the derivative of the self-consistent Kohn-Sham potential with respect to the atomic positions in the direction of mode displacement vector $\mathbf{u}_{\mathbf{q}\kappa}^{\nu}$, with $\kappa \equiv (\alpha, i)$ being the abbreviated index of atom α and direction $i = x, y, z$. We also evaluated the parameters

$$\lambda = 2 \int d\omega \frac{\alpha^2F(\omega)}{\omega}, \quad (3)$$

$$\omega_{ln} = \exp \left[\frac{2}{\lambda} \int d\omega \frac{\alpha^2F(\omega)}{\omega} \ln \omega \right], \quad (4)$$

$$\bar{\omega}_2 = \left[\frac{2}{\lambda} \int d\omega \frac{\alpha^2F(\omega)}{\omega} \omega^2 \right]^{\frac{1}{2}}, \quad (5)$$

which enter the McMillan-Allen-Dynes semiempirical formula for the superconducting transition temperature [35],

$$T_c^{\text{McM}} = f_1 f_2 \frac{\omega_{ln}}{1.2} \exp \left[-\frac{1.04(1 + \lambda)}{\lambda - \mu^*(1 + 0.62\lambda)} \right]. \quad (6)$$

The Coulomb pseudopotential μ^* represents the renormalized pair-breaking Coulomb repulsion [36,37]. The correction factors $f_1 = f_1(\lambda, \mu^*)$ and $f_2 = f_2(\lambda, \omega_{ln}, \bar{\omega}_2, \mu^*)$, which are both approximately unity in the weak-coupling limit, are defined in Ref. [35]. Finally we calculated the area under $\alpha^2F(\omega)$, A , which may better correlate with T_c than λ or ω_{ln} alone [38–40]:

$$A = \int d\omega \alpha^2F(\omega). \quad (7)$$

We adopted the Wannier representation of the electron-phonon coupling coefficient [41] for two purposes. First, we executed the efficient interpolation of $g_{n\mathbf{k}+\mathbf{q},n'\mathbf{k}}^{\nu\mathbf{q}}$ on dense \mathbf{k} and \mathbf{q} meshes for the convergence of the summations $\sum_{\nu\mathbf{q}} \sum_{n'n\mathbf{k}}$ in Eq. (1) using the inverse and forward Fourier transformations as formulated in Ref. [41]. Second, we performed decomposition of $\alpha^2F(\omega)$ into local electronic and phononic contributions. Namely,

$$\alpha^2F(\omega) = \frac{1}{N(0)} \sum_{\nu\mathbf{q}} \sum_{n'n\mathbf{k}} |g_{n\mathbf{k}+\mathbf{q},n'\mathbf{k}}^{\nu\mathbf{q}}|^2 \delta(\omega - \omega_{\nu\mathbf{q}}) \times \delta(\xi_{n\mathbf{k}+\mathbf{q}}) \delta(\xi_{n'\mathbf{k}}) \quad (8)$$

$$= \frac{1}{N(0)} \sum_{\nu\mathbf{q}} \sum_{n'\mathbf{k}} \sum_{\kappa\kappa'} \sum_{\substack{m_1 m_2 \\ m_3 m_4}} G_{n'n';m_1 m_2 m_3 m_4}^{\nu;\kappa\kappa'}(\mathbf{k}, \mathbf{q}) \times \delta(\omega - \omega_{\nu\mathbf{q}}) \delta(\xi_{n\mathbf{k}+\mathbf{q}}) \delta(\xi_{n'\mathbf{k}}). \quad (9)$$

Indices m_1 – m_4 run over the Wannier orbitals. Factor $G_{n'n';m_1 m_2 m_3 m_4}^{\nu;\kappa\kappa'}(\mathbf{k}, \mathbf{q})$ is defined as

$$G_{n'n';m_1 m_2 m_3 m_4}^{\nu;\kappa\kappa'}(\mathbf{k}, \mathbf{q}) \equiv [u_{\mathbf{q}\kappa}^{\nu} \tilde{g}_{m_1 \mathbf{k}+\mathbf{q}, m_2 \mathbf{k}}^{\kappa\mathbf{q}} U_{n m_1, \mathbf{k}+\mathbf{q}} U_{n' m_2, \mathbf{k}}^*] \times u_{\mathbf{q}\kappa'}^{\nu} \tilde{g}_{m_3 \mathbf{k}+\mathbf{q}, m_4 \mathbf{k}}^{\kappa'\mathbf{q}} U_{n m_3, \mathbf{k}+\mathbf{q}} U_{n' m_4, \mathbf{k}}^*. \quad (10)$$

Here, $u_{\mathbf{q}\kappa}^{\nu}$ denotes the displacement vector of mode $\nu\mathbf{q}$ with weights in inverse proportion to the square root of the atomic mass values and $U_{n m_1, \mathbf{k}}$ denotes the unitary transformation from the Bloch to Wannier space, as defined in Ref. [41].

Coefficient $\tilde{g}_{m\mathbf{k}+\mathbf{q},m'\mathbf{k}}^{\kappa\mathbf{q}}$ thus means the matrix element between the Bloch sums of the individual Wannier orbitals m and m' via the collective displacements of κ with wave vector \mathbf{q} . The unambiguous decompositions of the Eliashberg function is then defined from Eqs. (9) and (10) as

$$\alpha^2 F(\omega) = \sum_{\kappa\kappa'} \sum_{\substack{m_1 m_2 \\ m_3 m_4}} \alpha^2 F_{m_1 m_2 m_3 m_4}^{\kappa\kappa'}(\omega). \quad (11)$$

In this study, we calculated the electronic Wannier orbitals using a preliminary version of RESPACK [42–47] code, which is an implementation of the method proposed by Souza, Marzari, and Vanderbilt for entangled energy bands [48,49].

We perform calculations of the superconducting transition temperature T_c in two ways within the Eliashberg theory [31–33] with the Migdal approximation [34]. The first is the isotropic Eliashberg equations

$$Z(i\omega_n) = 1 + \frac{\pi T}{\omega_n} \sum_m' \frac{\omega_m}{R(i\omega_m)} \lambda(\omega_n - \omega_m), \quad (12)$$

$$\Delta(i\omega_n) = \frac{\pi T}{Z(i\omega_n)} \sum_m' \frac{\Delta(i\omega_m)}{R(i\omega_m)} [\lambda(\omega_n - \omega_m) - \mu^*], \quad (13)$$

$$R(i\omega_m) = \sqrt{\omega_m^2 + \Delta^2(i\omega_m)}, \quad (14)$$

$$\lambda(\omega_n - \omega_m) = 2 \int_0^\infty d\omega \frac{\omega \alpha^2 F(\omega)}{\omega^2 + (\omega_n - \omega_m)^2}, \quad (15)$$

where ω_n denotes the fermionic Matsubara frequency. Sum \sum_m' is limited by the cutoff $|\omega_m| \leq \omega_{\max}$. The effect of the renormalized Coulomb repulsion is represented by the parameter μ^* , which is conceptually a function of ω_{\max} but treated as an adjustable parameter. The problem of calculating the superconducting transition temperature from these equations is recast to the following eigenvalue problem with a transformed order parameter $\bar{\Delta}$ (Ref. [50]):

$$\rho \bar{\Delta}(i\omega_n) = T \sum_m' \left\{ \lambda(\omega_n - \omega_m) - \mu^* - \delta_{mn} \frac{|\tilde{\omega}_m|}{\pi T} \right\} \bar{\Delta}(i\omega_m) \quad (16)$$

with

$$\tilde{\omega}_n = \omega_n + \pi T \sum_m' \text{sgn} \omega_m \lambda(\omega_n - \omega_m). \quad (17)$$

TABLE I. Detailed settings for the calculations. The format of the \mathbf{k} and \mathbf{q} point grids obeys the convention of QUANTUM ESPRESSO, where the second lattice vector is taken to be the interlayer one. Subscript “1” for \mathbf{q} points denotes the mesh with displacement by half a grid step in the first and third directions for avoiding divergence at $\mathbf{q} = \Gamma$. The wave function and charge density cutoffs for the charge density and dynamical matrix calculations were set to 80 Ry and 320 Ry, respectively.

		Method or setting
Charge density	\mathbf{k}	(12 4 12)
	interpol.	Optimized tetrahedron [59]
Dynamical matrix	\mathbf{k}	(12 4 12)
	\mathbf{q}	(6 2 6)
Wannier functions	interpol.	Optimized tetrahedron [59]
	\mathbf{k}	(6 2 6)
	Initial guess of orbitals	Y-d, X-p, and C-sp
	Outer window (eV)	[−18.7, 21.3]
Eliashberg function	Inner (frozen) window (eV)	[−1.0, 1.0]
	\mathbf{k}^a	(36 12 36)
	\mathbf{q}^a	(18 6 18) ₁
Dielectric function	interpol.	Optimized tetrahedron [59]
	\mathbf{k} for bands crossing E_F^b	(18 6 18)
	\mathbf{k} for other bands	(6 2 6)
	\mathbf{q}	(6 2 6)
	unoccupied band num.	~227
	interpol.	Tetrahedron with the Rath-Freeman treatment [60]
DOS for phononic kernels	Plane wave cutoff	12.8 Ry
	\mathbf{k}	(27 9 27)
Eliashberg equations solution	interpol.	Tetrahedron with the Blöchl correction [61]
	Matsubara frequency cutoff ω_{\max}	$6 \times \omega_{\alpha^2 F}^c$
SCDFT gap function	unoccupied band num.	107
	\mathbf{k} for the electronic kernel	(6 2 6)
	\mathbf{k} for the KS energy eigenvalues	(27 9 27)
	N_s for bands crossing E_F	6000
	N_s for other bands	200
	Sampling error in T_c	~7%

^aElectron and phonon energy eigenvalues and matrix elements were calculated on these auxiliary grid points.

^bElectron energy eigenvalues were calculated on these auxiliary grid points.

^c $\omega_{\alpha^2 F}$ was taken to be the maximum phonon frequency below which the calculated $\alpha^2 F(\omega)$ values are nonzero.

T_c is then given by the condition $\rho(T_c) = 0$. The functional derivative $\delta T_c / \delta \alpha^2 F(\omega)$, showing at which frequency the coupling effect on T_c is most significant, is evaluated using $\rho(T)$ and $\tilde{\Delta}(i\omega_n)$ by the Bergmann-Rainer formula [50,51].

Finally, we evaluate the superconducting transition temperature with the gap equation from the density functional theory for superconductors [52,53]

$$\Delta_{nk} = -Z_{nk}\Delta_{nk} - \frac{1}{2} \sum_{n'k'} \mathcal{K}_{nk n'k'} \frac{\tanh[(\beta/2)E_{n'k'}]}{E_{n'k'}} \Delta_{n'k'}. \quad (18)$$

Here, β is the inverse temperature, Δ_{nk} is the gap function, and E_{nk} is defined as $E_{nk} = \sqrt{\xi_{nk}^2 + |\Delta_{nk}|^2}$. The exchange-correlation kernels $\mathcal{K} = \mathcal{K}^{\text{ph}} + \mathcal{K}^{\text{el}}$ and $Z = Z^{\text{ph}}$ quantitatively treat the interaction effects within the Migdal-Eliashberg theory. Notably, the retardation effect on the effective Coulomb repulsion is treated without any empirical parameter like μ^* . It is achieved approximately, instead of using the Matsubara frequency, with the Kohn-Sham energy dependencies of \mathcal{K}^{ph} and \mathcal{K}^{el} [52,53]. The $n\mathbf{k}$ -averaged forms for \mathcal{K}^{ph} (Eq. (23) in Ref. [53]) and Z^{ph} (Eq. (40) in Ref. [54]) were employed for the phononic terms, which can be calculated using the Eliashberg function $\alpha^2 F(\omega)$. The electronic term \mathcal{K}^{el} , which describes the screened Coulomb repulsion, was treated with the fully $n\mathbf{k}$ -dependent form: we adopted the formula of Eq. (3) in Ref. [55], in which the dielectric matrix within the random phase approximation is used for the plasmonic effect [56–58]. Those terms were evaluated using the normal-state properties as formulated in the above references.

In Table I we summarize the detail conditions of the electron, phonon, and superconducting calculations. We consistently employed the tetrahedron interpolation methods for the singular integrals such as Eq. (1), which, in contrast to the smearing methods, assured convergence to the exact integrals with efficient number of wave-number grid points.

III. RESULTS

A. Structural properties

The series of $\text{Y}_2\text{X}_2\text{C}_2$ compounds exhibit base-centered monoclinic lattice for all the cases $X = \text{Cl}, \text{Br}, \text{I}$ (Fig. 1). At ambient pressure, they crystallize in two slightly different stacking forms 1s and 3s, belonging to the same space group $C2/m$ (Fig. 2). These structures have the common X-Y-C₂-Y-X layers as the building blocks and are related by changing the interlayer lattice vectors. Their naming convention is based on the approximate periods in the vertical direction of some representative systems [16]. We comply with this convention in this paper, although we point out that the two types of stacking are more definitely distinguished by the positions of the neighboring halogen atoms [Figs. 2(a) and 2(b)]. The lower panels of Figs. 2(a) and 2(b) display this fact. The halogen atoms form distorted triangular nets indicated as L_1 and L_2 . Provided that the maximal symmetry is conserved, the relative position of the L_2 atoms can be either over the left- or right-directed triangles of L_1 , which correspond to 1s and 3s, respectively [63]. At ambient pressure the $X = \text{Cl}$ and I

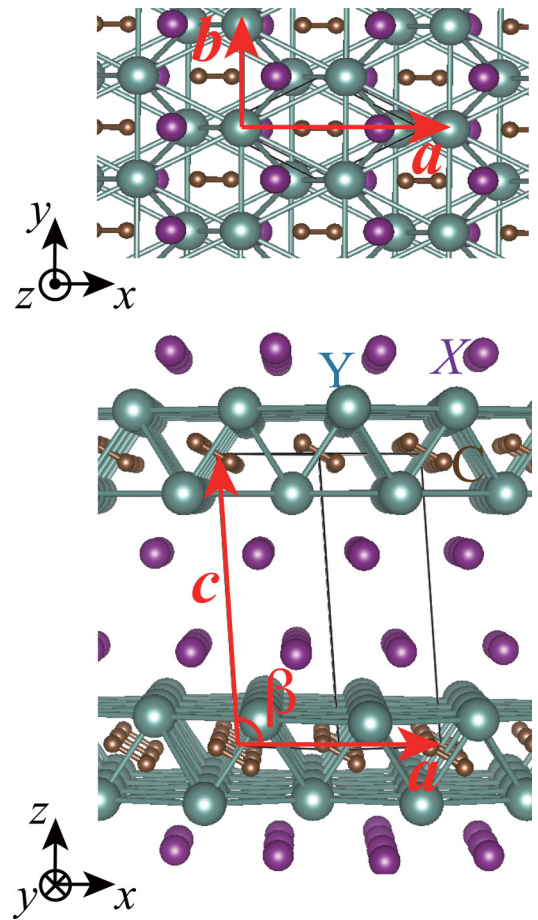


FIG. 1. Crystal structure of 1s- $\text{Y}_2\text{X}_2\text{C}_2$ with the lattice parameters, visualized by VESTA [62]. The monoclinic base-centered unit is shown by thin lines. (Upper) Top view of the X-Y-C₂-Y-X block and (lower) the perspective view of the whole structure.

systems take the 1s stacking whereas the $X = \text{Br}$ system takes the 3s stacking [16]. A previous first-principles simulation indicates that the formation energies of 1s and 3s stacking are very close [20]. We adopted the experimentally observed stacking forms as the initial conditions for the structure optimization. The optimized lattice parameters are summarized in Table II. We also list the optimized bonding lengths of the yttrium octahedra containing the carbon dimers [Fig. 2(c)] in Table III. The values show fair agreement with the experimental data. A systematic underestimation of the structural parameters by $\sim 2\%$ was observed, though it does not affect the discussion in this section.

As the halogen atoms are substituted from the lighter (Cl) to heavier (I), the optimized lattice vectors tend to become longer, especially in the interlayer direction c . Although this trend is a straightforward consequence of the difference in the halogen ionic radii, we also find its remarkable effect on the Y_2C_2 layered blocks. The distance between the upper and lower yttrium planes indicated as D in Fig. 2 decreases by 7% with substitution from Cl to I. This trend is contrary to the expansion of the lattice vectors. Previously, this unusual observation was attributed to the local distortion of the yttrium octahedra [23]. Here we suggest an alterna-

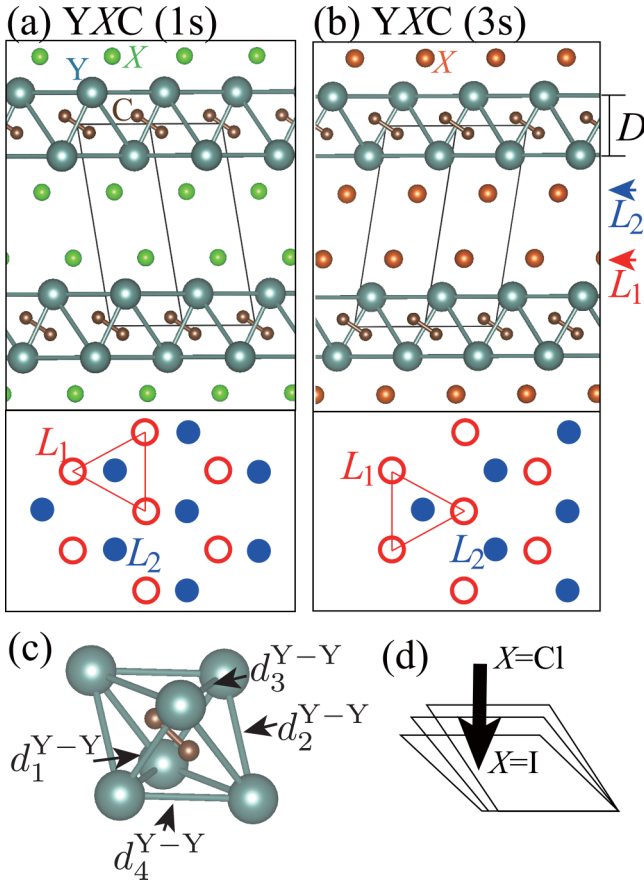


FIG. 2. Schematic illustration of the crystal structures of $Y_2X_2C_2$ with (a) 1s and (b) 3s stacking geometries. The definition of the yttrium interplane distance D is indicated. In the lower panels the top views of the neighboring halogen layers L_1 and L_2 are shown. (c) Yttrium octahedron containing the carbon dimer, the array of which forms the individual Y_2C_2 block layers. (d) Schematic of the Poisson-type structural change of the yttrium framework by the halogen substitution, where the degree of changes is exaggerated.

tive as a uniaxial compression and lateral expansion of the Y_2C_2 blocks [Fig. 2(d)]. It is, in fact, a microscopic Poisson effect where the halogen atoms exert on the blocks uniaxial pressure whose strength depends on their ionic radii. This perspective has apparently been obscured by the expansion of the lattice vectors. It is hence encouraged to revisit the experimental [16,64] and previous first-principles [23] data to see if this Poisson-type structural change of the yttrium framework is indeed presented.

B. Electronic properties

We next examine the halogen-atom dependence of the electronic band structure. The calculated band structures and density of states (DOS) are shown in Fig. 3. The most pronounced change in the band structure from the halogen substitution is the gap opening of the two nearly degenerate bands at the Γ point. The partial DOS spectra derived by the projection onto the Wannier orbitals indicate that the metallic bands are formed by the carbon- p and yttrium- d orbitals. This is consistent with the elementary molecular-orbital model [16] and previous first-principles calculations using localized basis

TABLE II. Optimized lattice parameters compared with the experimentally observed values [16].

	YCIC		YBrC		YIC	
	Calc.	Expt.	Calc.	Expt.	Calc.	Expt.
a (\AA)	6.761	6.820	6.872	6.953	7.114	7.212
b (\AA)	3.672	3.713	3.718	3.764	3.809	3.876
c (\AA)	9.453	9.327	9.914	9.938	10.205	10.411
β (deg)	95.31	94.75	99.49	99.98	93.80	93.55

sets [16,23]. The halogen- p states are consistently fully occupied, indicating an ionic character of the bonding between the halogen atoms and YC blocks. Their energy levels move upward by the substitution from the lighter to heavier ones, which reflects the change in the electron affinity.

The effects of the halogen atoms on the band structures can be divided into three contributions. The halogen atoms (i) exert internal uniaxial pressure which distorts the YC blocks, (ii) serve as sources of the one-body ionic potential for the YC metallic states, and (iii) provide local orbitals that mediate the interlayer hybridization across the YC blocks. To examine these contributions quantitatively, we calculated the band structures in hypothetical crystals where the halogen atoms are removed and compensating uniform charges are filled instead. Remarkably, the entire structures of the conduction bands of the original systems are well reproduced with these hypothetical crystals. This fact shows that the metallic properties are dominated by the YC layers and effect (ii) is small. We can see effect (i) on the YC layers from the changes from Figs. 3(e), 3(f) to 3(g). The bands at the Γ points are inverted with the halogen substitution. This is closely related to the shape of the Y-octahedron. In the chloride system $d_2^{Y-Y} > d_4^{Y-Y}$, whereas in the iodide $d_2^{Y-Y} < d_4^{Y-Y}$ [see Fig. 2(c) for the definition of the bonds]. The band inversion occurs through the crossover regime $d_2^{Y-Y} \simeq d_4^{Y-Y}$. From the comparison between Figs. 3(b) and 3(e), effect (ii) also contributes to this inversion. Effect (iii) results in a small band dispersion in the interlayer direction (Γ -A path), which is more noticeable in the iodide than in the chloride and bromide as expected from the degree of proximity of the halogen- p energy levels.

The band inversion observed in the above hypothetical structures implies an interesting possibility in the chloride system whose properties have been less explored before. Since the low-energy valence bands at Γ are nearly degenerate in the chloride, by exerting a uniaxial tensile strain on this, the difference $d_2^{Y-Y} - d_4^{Y-Y}$ is enlarged and a nonmonotonic change in its electronic characteristics may be observed due to the band inversion. The same would also be true for the bromide system, though the required strain should be stronger.

C. Phononic properties

We next examine the calculated phonon spectra shown in Fig. 4. The branches form three distinct groups; the low-frequency branches (less than 300 cm^{-1}), medium-range frequency branches (between 250 cm^{-1} and 500 cm^{-1}), and the single high-frequency mode. We refer to these branches

TABLE III. Optimized bond lengths characterizing the yttrium octahedron containing the carbon dimer compared with the experimentally observed values [16]. The second column shows the degree of degeneracy of the respective bonds. The interplane distances D as defined in Fig. 2 are also shown. All the values are in units of Å.

	$X = \text{Cl}$		$X = \text{Br}$		$X = \text{I}$	
	deg.	Calc.	Calc.	Expt.	Calc.	Expt.
$d_1^{\text{Y}-\text{Y}}$	1	3.372	3.356	3.400(6)	3.319	3.370(7)
$d_2^{\text{Y}-\text{Y}}$	2	3.899	3.854	3.764(1), 3.852(5)	3.771	3.726(6), 3.866(2)
$d_3^{\text{Y}-\text{Y}}$	2	3.675	3.719		3.811	
$d_4^{\text{Y}-\text{Y}}$	4	3.847	3.907	3.953	4.035	4.075(3)
Average		3.767	3.792	3.827	3.847	3.872
$d^{\text{C}-\text{C}}$		1.330	1.327	1.267(12)	1.322	1.304(6)
D (Å)		2.955	2.895		2.763	

and corresponding frequency ranges as “low,” “medium,” and “high” in the later discussions, respectively. From the analysis of the phonon DOS (right panels) and mode vectors, the lowest branches are dominated by the yttrium and halogen atoms whereas the medium-frequency branches correspond to the motions of the carbon dimers as a rigid body (three transla-

tions and two librations). The C-C stretch of the C_2 dimer has the highest frequency. These are consistent with the previous experimental characterization of the Raman-active modes [64] and first-principles simulation [23]. Note that the appearance of the dimer rigid-body vibrations at intermediate-frequency regimes is a feature common to YC_2 (Ref. [22]).

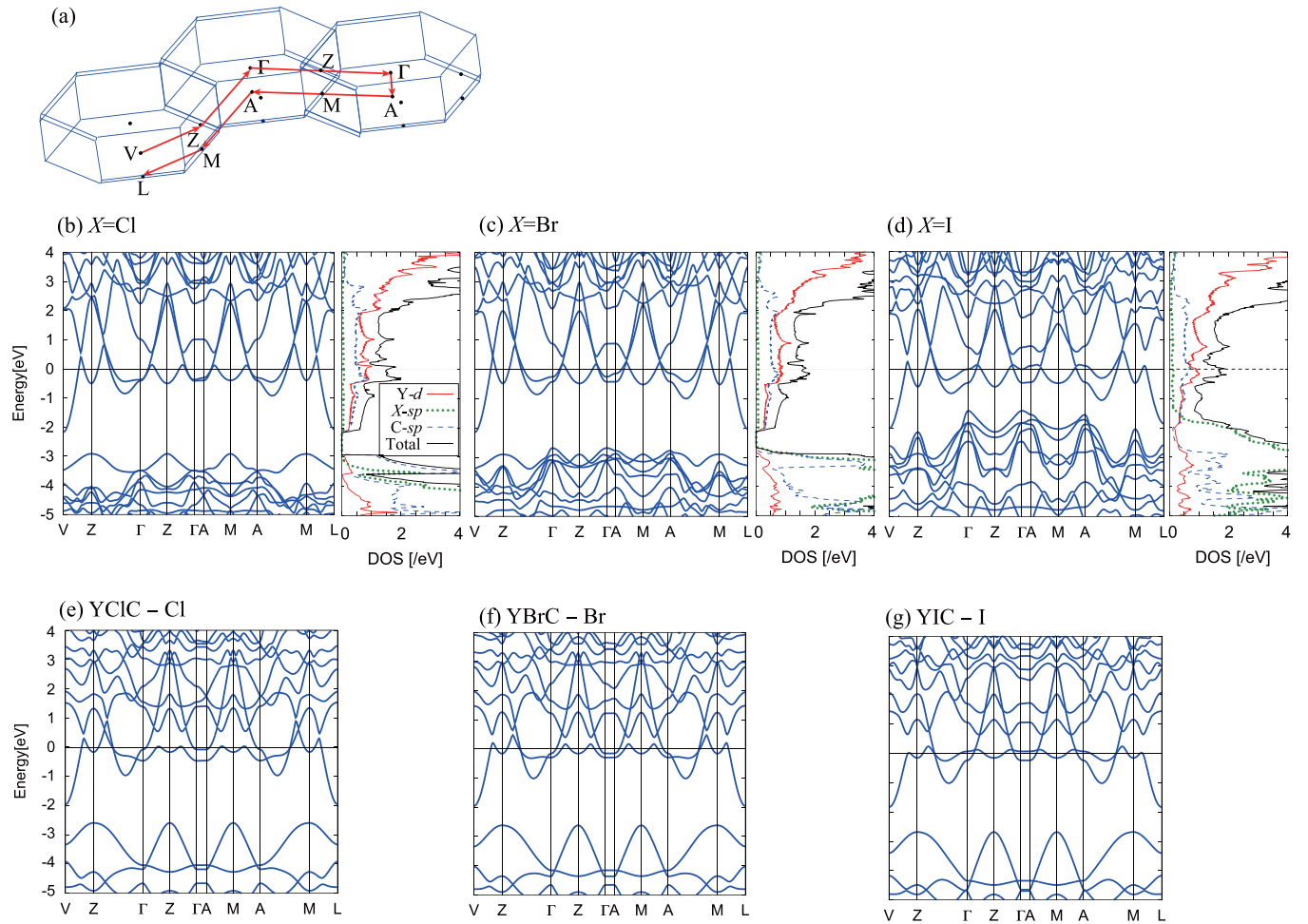


FIG. 3. Electronic band structures of $\text{Y}_2\text{X}_2\text{C}_2$. (a) The Brillouin zone and \mathbf{k} -point path. (b)–(d) Band structures, total DOS, and partial DOS spectra. (e)–(g) Band structures of the artificial systems $\text{Y}_2(e^-)_2\text{C}_2$ whose crystal structures were constructed by subtracting the halogen atoms from the optimized structures of the original stoichiometric systems.

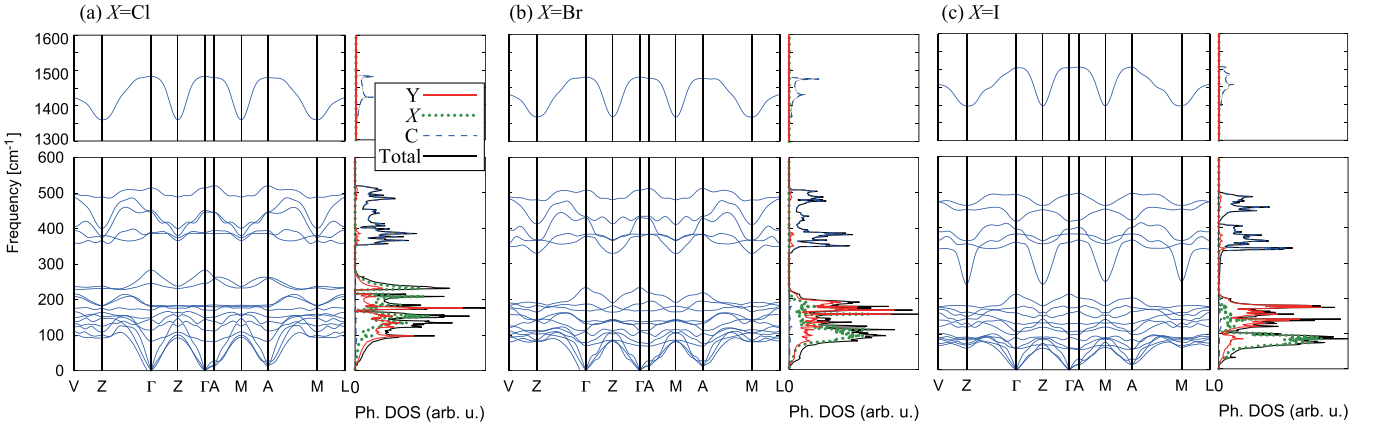


FIG. 4. Phonon dispersion and DOS of $Y_2X_2C_2$. The components of the phonon DOS projected onto the respective atoms are also shown.

We summarize the frequencies of the calculated Raman and infrared-active modes in Table IV. Except for the carbon dimer stretching mode, the present theoretical predictions agree well with the preceding experimental and first-principles results.

In the calculated phonon spectra in Fig. 4, we observe two significant halogen dependencies. First, the halogen-atom component of the projected vibrational DOS shifts downward in frequency with replacement of the lighter halogen by heavier atoms, which is a trivial consequence of the change in the atomic mass. Second, more strikingly, one of the carbon modes shows significant softening at the Z and M points by the halogen-atom substitution. This mode was found to be a collective libration of the carbon dimers as depicted in Fig. 5. This softening implies that the $1s$ - $Y_2I_2C_2$ having the highest T_c is on the verge of some structural instability related to this libration, which is apparently distinct from the $1s$ - $3s$ transition under pressure [20].

TABLE IV. Calculated phonon frequencies at Γ . The referenced experimental and first-principles calculation data are taken from Refs. [23,64], respectively.

	X = Cl		X = Br		X = I		
	Present	Present	Expt.	Calc.	Present	Expt.	Calc.
A_g	1483	1483	1593	1589	1503	1588	1527
A_g	451	432	436	436	398	401	403
A_g	284	233	236	232	213	215	219
A_g	172	169	166	172	174	169	173
A_g	144	109	108	113	91	93	94
A_g	114	79		79	62		59
B_g	446	436		436	420		421
B_g	181	138	140	131	130	126	128
B_g	83	70	67	66	59	58	58
A_u	386	386			384		
A_u	184	132			109		
B_u	514	513			491		
B_u	388	379			361		
B_u	246	187			161		
B_u	149	114			98		

D. Electron-phonon coupling properties and superconducting T_c

We show in Fig. 6 the calculated Eliashberg spectral function $\alpha^2F(\omega)$ ¹ and partially integrated $\lambda(\omega)$, which converges to λ [Eq. (3)] in the $\omega \rightarrow \infty$ limit, defined as

$$\lambda(\omega) = 2 \int_0^\omega d\omega' \frac{\alpha^2F(\omega')}{\omega'}. \quad (19)$$

For all the systems, approximately half of the total λ originates from the coupling of the lowest yttrium-halogen branches. Most of the remainder is from the translation and libration modes of the carbon dimers, whereas the contribution of the stretching mode is little. The large fraction of the yttrium-halogen contribution explains the not so appreciable isotope effect found in experiments [24]. The halogen dependence of the total λ (Table V) agrees well with the experimentally observed trend of T_c , with which we can actually reproduce the values of T_c from first principles in the right order as seen later. As the halogen atoms become heavier, the characteristic frequencies ω_{1n} and ω_2 monotonically decrease. The mechanism of this seems simply understandable from the change of the atomic mass, but below we find that the situation is not that obvious. The area A is almost constant. The relations of ω_{1n} , ω_2 and A to T_c are discussed below.

Here we elucidate the origin of the coupling with the local decompositions $\alpha^2F_{m_1m_2m_3m_4}^{\kappa\kappa'}(\omega)$ defined in Eq. (11). We first define a partial sum of them as

$$\alpha^2F_a^{\text{ph}}(\omega) = \sum_{\kappa, \kappa' \in a} \sum_{m_1m_2m_3m_4} \alpha^2F_{m_1m_2m_3m_4}^{\kappa\kappa'}(\omega). \quad (20)$$

The operation $\sum_{\kappa, \kappa' \in a}$ denotes the partial sum for the displacement κ and κ' corresponding to the atomic kind a ($=Y, X, C$). This function indicates the partial contribution to $\alpha^2F(\omega)$ of the vibrations of the specific atoms. Similarly, we

¹To avoid the numerical instability due to artificial softening in an acoustic branch near the Γ point (Fig. 4), contribution from the phonon states with $\omega_{\text{vq}} < 40\text{cm}^{-1}$ was ignored in Eq. (1) for all the systems.

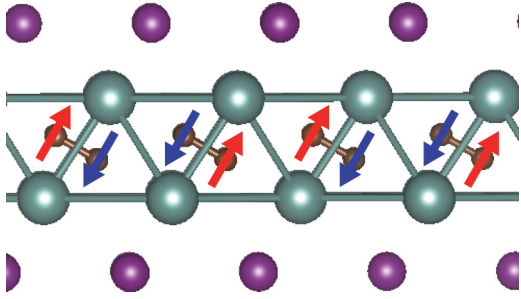


FIG. 5. Side view of the softened carbon dimer libration mode at Z and M in $Y_2I_2C_2$, where the mode Bloch phase in the layer direction is reflected.

also define another partial sum as

$$\alpha^2 F_b^{\text{el}}(\omega) = \sum_{m_1 m_2 m_3 m_4 \in b} \sum_{\kappa, \kappa'} \alpha^2 F_{m_1 m_2 m_3 m_4}^{\kappa \kappa'}(\omega). \quad (21)$$

The sum $\sum_{m_1 m_2 m_3 m_4 \in b}$ runs over the specific group of Wannier orbitals b and extracts the contributions of the target Wannier orbitals. The corresponding partial contributions to λ are defined as λ_a^{ph} and λ_b^{el} , respectively.

Figure 7 displays $\alpha^2 F_a^{\text{ph}}$ for $a = Y, X, C$. An important finding is that the component $a = X$ is negligibly small. The low-frequency branches are formed by entangled vibrations of yttrium and halogen atoms and from the total $\alpha^2 F$ we cannot see which kind of atoms mainly contribute: Our results clarify that the electron scattering processes due to the vibrations of halogen atoms are irrelevant. The partial λ^{ph} in Table V indicates that the contributions of the yttrium and carbon vibrations are of equal importance. Here, the reduction of ω_{in} and ω_2 by the halogen substitution from Cl, Br to I (Table V) is revealed to be an indirect effect which cannot be attributed to the coupling of the halogen-atom vibrations. As mentioned in Sec. III A, the substitution

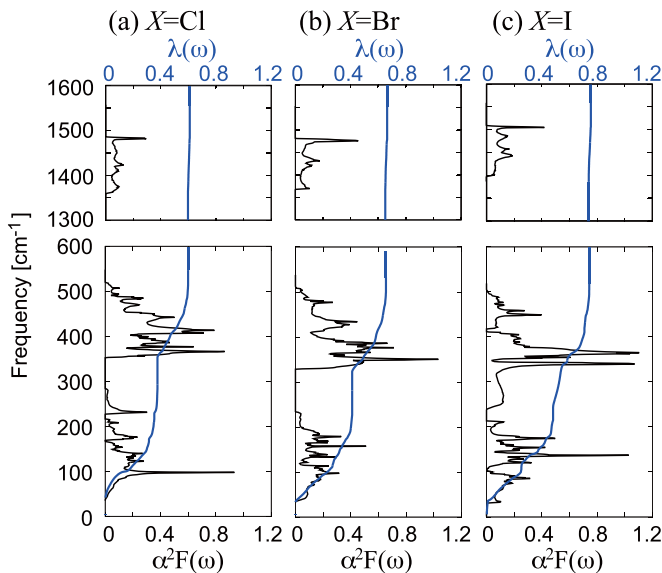


FIG. 6. Eliashberg spectral function $\alpha^2 F$ and partially integrated $\lambda(\omega)$ defined in Eq. (19) for $Y_2X_2C_2$.

TABLE V. Parameters representing the phonon mediated pairing and superconducting transition temperatures from first principles. See text for the definitions of λ^{ph} .

	YCIC	YBrC	YIC
$N(0)$ [(eV sp) $^{-1}$]	0.781	0.803	0.859
λ	0.610	0.667	0.755
λ_Y^{ph}	0.288	0.271	0.319
λ_C^{ph}	0.314	0.360	0.484
ω_{in} (K)	273	244	224
ω_2 (K)	489	468	448
A (K)	111	114	119
T_c^{McM} ($\mu^* = 0.13$) (K)	4.7	5.6	7.3
T_c^{SCDFT} (K)	2.6	3.3	4.6
T_c^{exp} (K)	2.3	5.0	10.0

of the halogen atoms induces the uniaxial compression of the Y_2C_2 blocks. This results in softening of the C_2 libration modes strongly coupled to the conducting electrons and downward shift of the medium-range frequency component of $\alpha^2 F(\omega)$.

In Fig. 8, we show $\alpha^2 F_b^{\text{el}}$ for $b = \{Y-d, C-sp\}$, $\{Y-d\}$, and $\{C-sp\}$. The components involving the $X-sp$ orbitals are presumably negligible according to the small projected DOS in Fig. 3. We note that the $b = \{Y-d, C-sp\}$ component reproduces the total $\alpha^2 F$ almost completely, whereas the $b = \{Y-d\}$ and $b = \{C-sp\}$ components are much smaller. In the later two, electron scattering processes across the $Y-d$ and $C-sp$ orbitals are ignored. These ignored processes are thus found to be essential for reproducing the total $\alpha^2 F$ and, in particular, the small $b = \{C-sp\}$ component directly demonstrates that the Zintl-Klemm pairing theory, or the “ C_2 units as pairing traps” scenario of Simon [18] does not simply apply.

We thus clarified origins of the three major branches of the $\alpha^2 F(\omega)$ spectra. To understand their effects on T_c , we solved the transformed Eliashberg equation Eq. (16) and calculated T_c with modifications to the input $\alpha^2 F(\omega)$ so that it

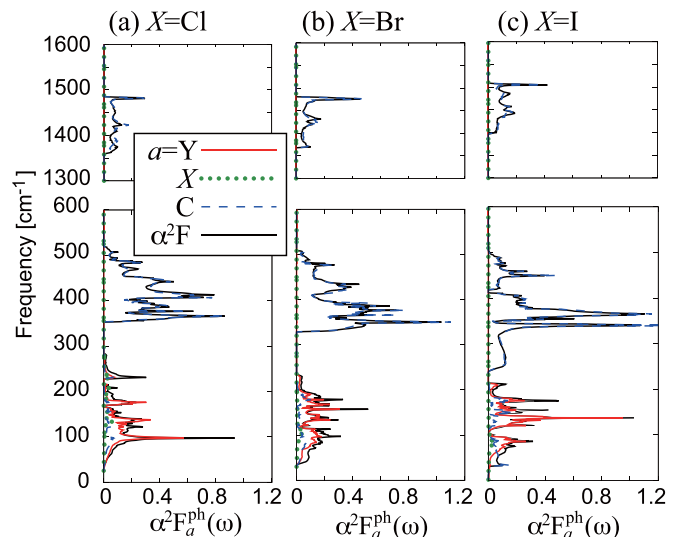


FIG. 7. Partially summed components of the Eliashberg function defined in Eq. (20).

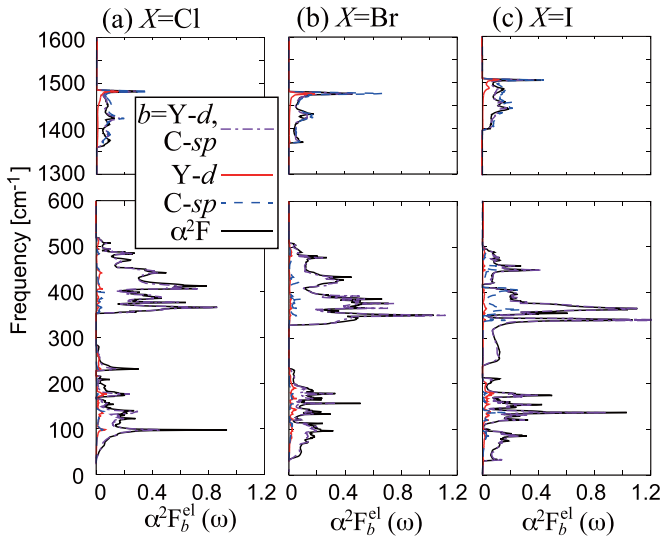


FIG. 8. Partially summed components of the Eliashberg function defined in Eq. (21).

is suppressed to zero at certain frequency ranges. The values of T_c with varying the empirical Coulomb parameter μ^* are shown in Fig. 9. By suppressing its amplitude to zero for the high-frequency branch, the resulting T_c values are lowered only by ~ 1 K (“all” to “low-medium”), which indicates the small coupling effect of the carbon stretching modes. If we further suppress either of the low and medium frequency branches (from “low-medium” to “medium” or “low”), T_c significantly decreases. The later result shows that the origin of the observed T_c s cannot be attributed solely to either of the carbon rigid modes or yttrium modes.

In the above calculations, the values of T_c were qualitative estimates because of the undetermined empirical value μ^* . We finally solved the SCDFT gap equation [Eq. (18)] using the calculated $\alpha^2 F$ and other electronic normal-state properties and evaluated T_c s nonempirically. The resulting values in Table V reproduce the experimentally observed halogen dependence: $T_c(X = \text{Cl}) < T_c(X = \text{Br}) < T_c(X = \text{I})$. This result indicates that the Migdal-Eliashberg picture is valid for describing superconductivity in this series of compounds. We note that T_c of $\text{Y}_2\text{I}_2\text{C}_2$ is significantly underestimated. The discrepancy may be a hint that physics beyond the Migdal-Eliashberg theory should become relevant in this system. Here we stress a possible importance of the softened C_2 libration mode in Fig. 5. Despite the small phonon DOS seen in Fig. 4, this branch has contribution by ~ 0.1 to the total λ . It is hence inferred that the electron scattering strength of the libration mode [represented by $\alpha^2 F/(\text{phonon DOS})$] is anomalously large. Higher-order vertex corrections involving this mode can have appreciable effect or, more drastically, charge density wave fluctuations induced by the strong interaction might partially break the conventional pairing picture.

The halogen dependence of the calculated T_c well conforms to that derived from the semiempirical McMillan-Allen-Dynes formula T_c^{McM} [(Eq. 6); Table V]. We can therefore interpret the origin of the increase of T_c upon the halogen substitution with the parameters entering the formula. In terms of λ , ω_{ln} , and ω_2 , it is due to the enhancement

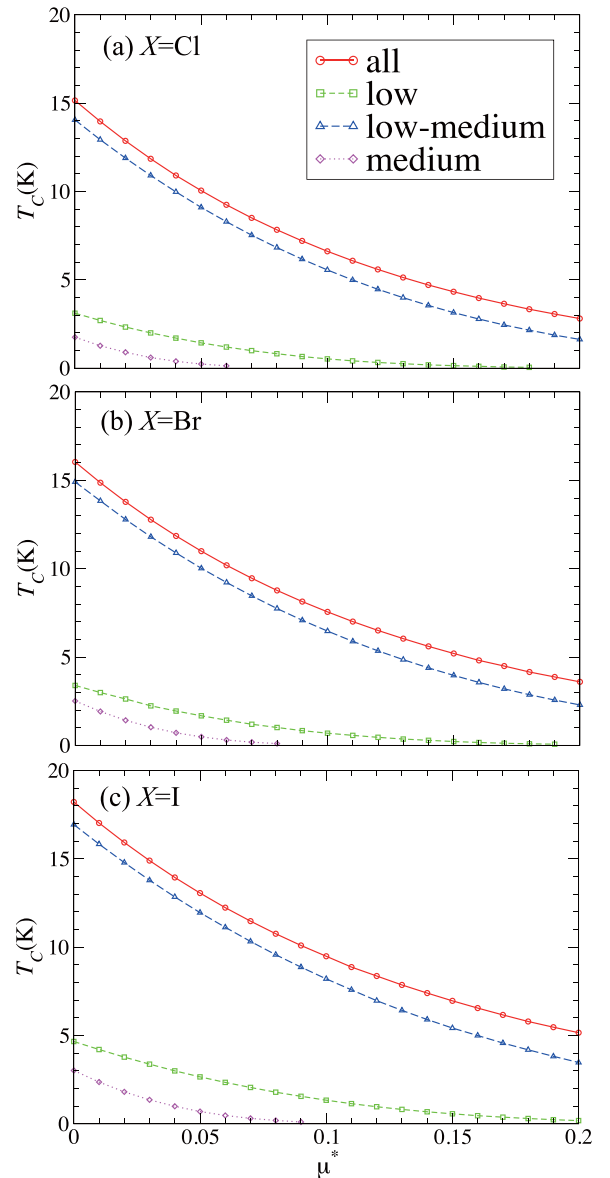


FIG. 9. Transition temperatures calculated by the Eliashberg equations with varying Coulomb repulsion parameter μ^* . Legends indicate the frequency ranges where input $\alpha^2 F(\omega)$ is kept to nonzero.

of λ dominating over the reduction of ω_{ln} and ω_2 . Another interpretation is derived by focusing on the almost constant area A. We show in Fig. 10 the calculated functional derivative $\delta T_c / \delta \alpha^2 F(\omega)$ for T_c derived from the Eliashberg equation. The functional derivative takes its maximum value for all the three systems at $\lesssim 50 \text{ cm}^{-1} \simeq 70 \text{ K}$, which is consistent with the preceding studies where the maximum was observed at $\omega \sim 7T_c$ [39,51,65]. With A kept constant, T_c is therefore raised by concentration of $\alpha^2 F(\omega)$ around $7T_c \sim 50 \text{ cm}^{-1}$. In this respect, the smaller ω_{ln} and ω_2 are more advantageous for T_c in $\text{Y}_2\text{X}_2\text{C}_2$, which is why T_c increases despite the decrease of those frequencies. In other words, $\text{Y}_2\text{I}_2\text{C}_2$ hosts the optimum distribution of $\alpha^2 F$ among the halides with a given total area under it.

Although we reproduced the proper halogen dependence of T_c , why the distortion of the Y_2C_2 blocks induced by the

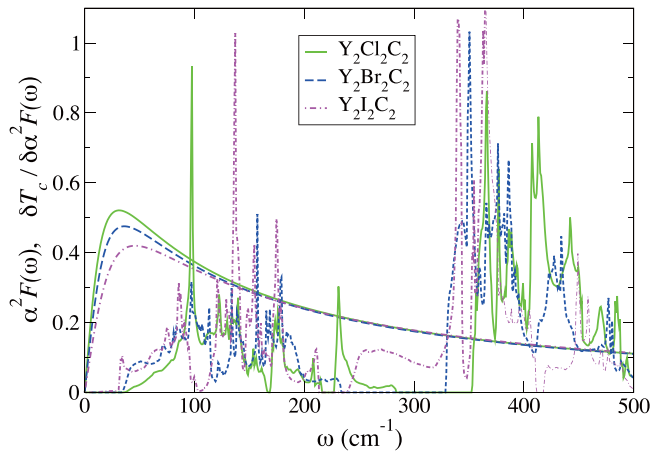


FIG. 10. Functional derivative of T_c with respect to $\alpha^2 F(\omega)$ with the $\alpha^2 F(\omega)$ spectra. The empirical parameter μ^* was set to 0.13.

halogen substitution results in the change of T_c is not as simple according to the present calculations. The electronic DOS at the Fermi energy $N(0)$, to which the total coupling λ is approximately proportional, shows a slight increase by halogen substitution from the lighter to heavier atoms as pointed out in the previous first principles band structure calculation [23]. However, it does not completely explain the enhancement of the total λ . Thus, in this work, we stop with the remark that the distortion of the Y_2C_2 blocks induces the enhancement of the electron-phonon matrix elements as well as the slight increase of the DOS. A more detailed theory on how the distortion affects the electron-phonon coupling is left for future studies.

IV. DISCUSSIONS AND SUMMARY

Through first-principles calculations of the structural and electron-phonon properties, we established an understanding of superconductivity in the yttrium carbide halide. The Wannier-based analyses of the electron-phonon coupling have revealed that the mechanism of the T_c change by the halogen substitution is rather indirect. The halogen ions affect the pairing solely via the local uniaxial compressive force distorting the Y_2C_2 blocks of the Poisson type, which induces changes in the low-energy electronic band structure, phonon spectra of the Y-X entangled vibrations, and electron-phonon coupling character in the blocks. Neither their electronic orbitals nor ionic displacements directly participate in the superconducting pairing mechanism. Within the superconducting Y_2C_2 blocks, rigid-body vibrations of the carbon dimers and vibrations of the yttrium frameworks containing them are energetically well decoupled, but both have appreciable contributions to the total pairing. We cannot attribute the pairing electrons to either Y- d or C- sp electronic orbitals since the scattering processes across them are essential. In that sense, the Y- d or C- sp orbitals are entangled from the electron-phonon coupling aspect. The simple perspective with emphasis on the C_2 molecular orbitals is hence invalid. The coupling of the C_2 bond stretching mode is, contrary to the expectation, small and have little effect on T_c : Its values of order 1–10 K is due to the moderately high frequencies of the C_2 rigid-body modes interacting with both the Y- d and C- sp

orbitals. The irrelevance and relevance of those C_2 modes are common to yttrium sesquicarbide Y_2C_3 (Ref. [21]).

According to the calculated values of T_c and electron-phonon coupling parameters, the halogen-atom dependence of T_c is due to the difference of the electron-phonon matrix elements within the Y_2C_2 blocks, not only of the electronic DOS at the Fermi energy, although direct explanation as to how they occur upon the structural Poisson effect is left for future studies. In the most distorted iodide system, anomalous frequency softening of the collective carbon libration mode has been observed, with which the calculated T_c with the phonon-mediated SCDFT substantially departs from the experimentally observed value. Because this softening is accompanied by the enhancement of the corresponding electron-phonon coupling matrix element, it may have effects beyond the Migdal-Eliashberg picture. The $Y_2I_2C_2$ system hence serves as a testbed for quantitative numerical methods for unconventional mechanisms. Recently, the quantitative difference between the nonempirical Eliashberg theory [66] and SCDFT was examined [67]. With the results therein, a possibility arises that the improvement of the SCDFT kernels for the phonon pairing [67] may correct the current underestimation of T_c for the bromide and iodide to some extent: This is also an important issue for testing the applicability of the conventional phonon-mediated mechanism.

Apart from the mechanism, the remarkable correlation between the Poisson distortion of the Y_2C_2 blocks and T_c suggests an interesting path to higher T_c . Namely, a uniaxial compression of the system may enhance the distortion of the yttrium frameworks. In a previous experiment, hydrostatic pressure was exerted on $Y_2I_2C_2$ (Refs. [20,68]). There, enhancement of T_c up to 11.5 K was observed at the critical pressure where the stacking changes from 1s to 3s. A similar enhancement was observed with partial halogen substitution in $Y_2(\text{Br}, \text{I})_2C_2$ (Refs. [16,19]). They probably originated from the structural instability on the verge of the 1s-3s phase transformation. The uniaxial pressure, which is expected to further soften the carbon libration mode, may drive the system toward another structural instability. The carbon libration modes should then be “mixed (Ref. [69])” with the yttrium modes and the distribution of $\alpha^2 F(\omega)$ becomes more concentrated around $\sim 7T_c$, close to the optimal condition for T_c .

Lastly, we note the potential generality of the concept of internal structural compression generated by the halogen atoms. The effect of replacing the atoms within the same group is interpreted as the change of the radii of the ions at the corresponding positions. The point is that, in compounds containing two or more kinds of atoms, the stress induced by varying the atomic radii is generally nonuniform. It can therefore induce expansion of a certain structure and compression of another simultaneously. In the current $Y_2X_2C_2$ system (and probably in other layered systems), the replacement of the intercalant ions was found to induce the uniaxial compression and lateral expansion of the superconducting blocks, which cannot be directly inferred from the change of the monotonically increasing lattice parameters. More generally, one would find a variety of structural deformations induced by the nonuniform electronic stress, which will provide us with a novel method of controlling the properties of materials in addition to exerting external pressures.

ACKNOWLEDGMENTS

R.Ak. thanks Mitsuaki Kawamura and Yusuke Nomura for providing subroutines for the tetrahedron integrations of the Eliashberg function and calculation of the electron-phonon matrix elements in the Wannier gauge, respectively. This work was supported by JSPS KAKENHI Grants No. 15K20940 (R.Ak.) and No. 19H05825 (R.Ar.) from the Japan Society for the Promotion of Science (JSPS) and by the Natural Sciences and Engineering Research Council of

Canada (K.T. and J.S.T.). C.Z. acknowledges financial support from the National Natural Science Foundation of China (Grant No. 11874318) and the Natural Science Foundation of Shandong Province (Grant No. ZR2018MA043). J.S.T. wishes to thank Compute Canada for the allocation of computing resources. Some calculations were performed at the Supercomputer Center at the Institute for Solid State Physics in the University of Tokyo and the SGI Rackable C2112-4GP3/C1102-GP8 (Reedbush-U/H/L) in the Information Technology Center, The University of Tokyo.

- [1] J. Bardeen, L. N. Cooper, and J. R. Schrieffer, *Phys. Rev.* **106**, 162 (1957).
- [2] J. Bardeen, L. N. Cooper, and J. R. Schrieffer, *Phys. Rev.* **108**, 1175 (1957).
- [3] Y. Li, J. Hao, H. Liu, Y. Li, and Y. Ma, *J. Chem. Phys.* **140**, 174712 (2014).
- [4] D. Duan, Y. Liu, F. Tian, D. Li, X. Huang, Z. Zhao, H. Yu, B. Liu, W. Tian, and T. Cui, *Sci. Rep.* **4**, 6968 (2014).
- [5] H. Liu, I. I. Naumov, R. Hoffmann, N. W. Ashcroft, and R. J. Hemley, *Proc. Natl. Acad. Sci. USA* **114**, 6990 (2017).
- [6] A. P. Drozdov, M. I. Erements, I. A. Troyan, V. Ksenofontov, and S. I. Shylin, *Nature (London)* **525**, 73 (2015).
- [7] M. Somayazulu, M. Ahart, A. K. Mishra, Z. M. Geballe, M. Baldini, Y. Meng, V. V. Struzhkin, and R. J. Hemley, *Phys. Rev. Lett.* **122**, 027001 (2019).
- [8] A. P. Drozdov, P. P. Kong, V. S. Minkov, S. P. Besedin, M. A. Kuzovnikov, S. Mozaffari, L. Balicas, F. F. Balakirev, D. E. Graf, V. B. Prakapenka, E. Greenberg, D. A. Knyazev, M. Tkacz, and M. I. Erements, *Nature (London)* **569**, 528 (2019).
- [9] A. R. Oganov, O. Isayev, A. Shapeev, P. Sushko, C. Gatti, A. Walsh, R. Akashi, X.-Q. Chen, R. R., V. Stevanovich, J.-F. Halet, A. Enyashin, O. Yazyev, and A. Aspuru-Guzik, *Computational Materials Discovery*, edited by A. R. Oganov, G. Saleh, and A. G. Kvashnin, (RSC Publishing, Cambridge, England, 2018).
- [10] J. A. Flores-Livas, L. Boeri, A. Sanna, G. Profeta, R. Arita, and M. Erements, *Phys. Rep.* **856**, 1 (2020).
- [11] A. Giorgi, E. Szklarz, M. Krupka, and N. Krikorian, *J. Less-Common Met.* **17**, 121 (1969).
- [12] M. Krupka, A. Giorgi, N. Krikorian, and E. Szklarz, *J. Less-Common Met.* **19**, 113 (1969).
- [13] G. Amano, S. Akutagawa, T. Muranaka, Y. Zenitani, and J. Akimitsu, *J. Phys. Soc. Jpn.* **73**, 530 (2004).
- [14] A. Giorgi, E. Szklarz, M. Krupka, T. Wallace, and N. Krikorian, *J. Less-Common Met.* **14**, 247 (1968).
- [15] T. Gulden, R. W. Henn, O. Jepsen, R. K. Kremer, W. Schnelle, A. Simon, and C. Felser, *Phys. Rev. B* **56**, 9021 (1997).
- [16] A. Simon, A. Yoshiasa, M. Bäcker, R. W. Henn, C. Felser, R. K. Kremer, and H. Mattausch, *Z. Anorg. Allg. Chem.* **622**, 123 (1996).
- [17] R. W. Henn, W. Schnelle, R. K. Kremer, and A. Simon, *Phys. Rev. Lett.* **77**, 374 (1996).
- [18] A. Simon, *Angew. Chem., Int. Ed. Engl.* **36**, 1788 (1997).
- [19] R. Henn, K. Ahn, H.-A. von Nidda, R. Kremer, and A. Simon, *Physica C* **341-348**, 719 (2000).
- [20] K. Ahn, R. K. Kremer, A. Simon, W. G. Marshall, and A. Muñoz, *J. Phys.: Condens. Matter* **28**, 375703 (2016).
- [21] D. J. Singh and I. I. Mazin, *Phys. Rev. B* **70**, 052504 (2004).
- [22] J. Xue, Y. Guo, C. Liu, X. Sun, W. Qiu, S. Sun, and X. Ke, *Comput. Mater. Sci.* **159**, 120 (2019).
- [23] P. Puschnig, C. Ambrosch-Draxl, R. W. Henn, and A. Simon, *Phys. Rev. B* **64**, 024519 (2001).
- [24] W. Schnelle, R. W. Henn, T. Gulden, R. K. Kremer, and A. Simon, *J. Appl. Phys.* **83**, 7321 (1998).
- [25] P. Giannozzi, S. Baroni, N. Bonini, M. Calandra, R. Car, C. Cavazzoni, D. Ceresoli, G. L. Chiarotti, M. Cococcioni, I. Dabo, A. D. Corso, S. de Gironcoli, S. Fabris, G. Fratesi, R. Gebauer, U. Gerstmann, C. Gougoussis, A. Kokalj, M. Lazzeri, L. Martin-Samos *et al.*, *J. Phys.: Condens. Matter* **21**, 395502 (2009).
- [26] P. Hohenberg and W. Kohn, *Phys. Rev.* **136**, B864 (1964).
- [27] W. Kohn and L. J. Sham, *Phys. Rev.* **140**, A1133 (1965).
- [28] N. Troullier and J. L. Martins, *Phys. Rev. B* **43**, 1993 (1991).
- [29] J. P. Perdew, A. Ruzsinszky, G. I. Csonka, O. A. Vydrov, G. E. Scuseria, L. A. Constantin, X. Zhou, and K. Burke, *Phys. Rev. Lett.* **100**, 136406 (2008).
- [30] S. Baroni, S. de Gironcoli, A. Dal Corso, and P. Giannozzi, *Rev. Mod. Phys.* **73**, 515 (2001).
- [31] G. M. Eliashberg, *Zh. Eksp. Teor. Fiz.* **38**, 966 (1960) [*Sov. Phys. JETP* **11**, 696 (1960)].
- [32] D. J. Scalapino in, *Superconductivity*, edited by R. D. Parks, (Dekker, New York, 1969).
- [33] J. R. Schrieffer, *Theory of Superconductivity* (Westview, Boulder, CO, 1971).
- [34] A. B. Migdal, *Zh. Eksp. Teor. Fiz.* **34**, 1438 (1958) [*Sov. Phys. JETP* **7**, 996 (1958)].
- [35] P. B. Allen and R. C. Dynes, *Phys. Rev. B* **12**, 905 (1975).
- [36] P. Morel and P. W. Anderson, *Phys. Rev.* **125**, 1263 (1962).
- [37] W. L. McMillan, *Phys. Rev.* **167**, 331 (1968).
- [38] C. R. Leavens and J. P. Carbotte, *J. Low Temp. Phys.* **14**, 195 (1974).
- [39] J. P. Carbotte, *Rev. Mod. Phys.* **62**, 1027 (1990).
- [40] Y. Quan, S. S. Ghosh, and W. E. Pickett, *Phys. Rev. B* **100**, 184505 (2019).
- [41] F. Giustino, M. L. Cohen, and S. G. Louie, *Phys. Rev. B* **76**, 165108 (2007).
- [42] K. Nakamura, Y. Nohara, Y. Yosimoto, and Y. Nomura, *Phys. Rev. B* **93**, 085124 (2016).
- [43] K. Nakamura, Y. Yoshimoto, T. Kosugi, R. Arita, and M. Imada, *J. Phys. Soc. Jpn.* **78**, 083710 (2009).

- [44] K. Nakamura, R. Arita, and M. Imada, *J. Phys. Soc. Jpn.* **77**, 093711 (2008).
- [45] Y. Nohara, S. Yamamoto, and T. Fujiwara, *Phys. Rev. B* **79**, 195110 (2009).
- [46] T. Fujiwara, S. Yamamoto, and Y. Ishii, *J. Phys. Soc. Jpn.* **72**, 777 (2003).
- [47] K. Nakamura, Y. Yoshimoto, Y. Nomura, T. Tadano, M. Kawamura, T. Kosugi, K. Yoshimi, T. Misawa, and Y. Motoyama, *Comput. Phys. Commun.* **261**, 107781 (2021).
- [48] N. Marzari and D. Vanderbilt, *Phys. Rev. B* **56**, 12847 (1997).
- [49] I. Souza, N. Marzari, and D. Vanderbilt, *Phys. Rev. B* **65**, 035109 (2001).
- [50] Y. Yao, J. S. Tse, K. Tanaka, F. Marsiglio, and Y. Ma, *Phys. Rev. B* **79**, 054524 (2009).
- [51] G. Bergmann and D. Rainer, *Z. Phys.* **263**, 59 (1973).
- [52] M. Lüdgers, M. A. L. Marques, N. N. Lathiotakis, A. Floris, G. Profeta, L. Fast, A. Continenza, S. Massidda, and E. K. U. Gross, *Phys. Rev. B* **72**, 024545 (2005).
- [53] M. A. L. Marques, M. Lüdgers, N. N. Lathiotakis, G. Profeta, A. Floris, L. Fast, A. Continenza, E. K. U. Gross, and S. Massidda, *Phys. Rev. B* **72**, 024546 (2005).
- [54] R. Akashi and R. Arita, *Phys. Rev. B* **88**, 014514 (2013).
- [55] R. Akashi, M. Kawamura, S. Tsuneyuki, Y. Nomura, and R. Arita, *Phys. Rev. B* **91**, 224513 (2015).
- [56] Y. Takada, *J. Phys. Soc. Jpn.* **45**, 786 (1978).
- [57] R. Akashi and R. Arita, *Phys. Rev. Lett.* **111**, 057006 (2013).
- [58] R. Akashi and R. Arita, *J. Phys. Soc. Jpn.* **83**, 061016 (2014).
- [59] M. Kawamura, Y. Gohda, and S. Tsuneyuki, *Phys. Rev. B* **89**, 094515 (2014).
- [60] J. Rath and A. J. Freeman, *Phys. Rev. B* **11**, 2109 (1975).
- [61] P. E. Blöchl, O. Jepsen, and O. K. Andersen, *Phys. Rev. B* **49**, 16223 (1994).
- [62] K. Momma and F. Izumi, *J. Appl. Crystallogr.* **44**, 1272 (2011).
- [63] The apparently unstable structure where L_2 is exactly on top of L_1 is neglected here.
- [64] R. W. Henn, T. Strach, R. K. Kremer, and A. Simon, *Phys. Rev. B* **58**, 14364 (1998).
- [65] A. E. Karakozov, E. G. Maksimov, and S. A. Mashkov, *Zh. Eksp. Teor. Fiz.* **68**, 1937 (1975) [*Sov. Phys. JETP* **41**, 971 (1976)].
- [66] A. Sanna, J. A. Flores-Livas, A. Davydov, G. Profeta, K. Dewhurst, S. Sharma, and E. K. Gross, *J. Phys. Soc. Jpn.* **87**, 65 (2018).
- [67] A. Sanna, C. Pellegrini, and E. K. U. Gross, *Phys. Rev. Lett.* **125**, 057001 (2020).
- [68] K. Ahn, R. K. Kremer, A. Simon, W. G. Marshall, P. Puschnig, and C. Ambrosch-Draxl, *J. Phys.: Condens. Matter* **17**, S3121 (2005).
- [69] K. Tanaka, J. S. Tse, and H. Liu, *Phys. Rev. B* **96**, 100502(R) (2017).